C. R. Mecanique 346 (2018) 1033–1042

Contents lists available at ScienceDirect

Comptes Rendus Mecanique

www.sciencedirect.com

Computational methods in welding and additive manufacturing/Simulation numérique des procédés de soudage et de fabrication additive

Approaches in computational welding mechanics applied to additive manufacturing: Review and outlook

Lars-Erik Lindgren *, Andreas Lundbäck

Department of Engineering Sciences and Mathematics, Luleå University of Technology, 971 87 Luleå, Sweden

ARTICLE INFO

Article history:
Received 19 February 2018
Accepted 12 April 2018
Available online 20 August 2018

Keywords:
Simulations
Welding
Additive manufacturing
Microstructure
Thermo-mechanics

ABSTRACT

The development of computational welding mechanics (CWM) began more than four decades ago. The approach focuses on the region outside the molten pool and is used to simulate the thermo-metallurgical-mechanical behaviour of welded components. It was applied to additive manufacturing (AM) processes when they were known as weld repair and metal deposition. The interest in the CWM approach applied to AM has increased considerably, and there are new challenges in this context regarding welding. The current state and need for developments from the perspective of the authors are summarised in this study.

1. Introduction

Additive manufacturing (AM) describes various techniques for building a three-dimensional (3D) geometry in a layer-by-layer fashion. Powder bed fusion (PBF) and directed energy deposition (DED) are common examples of AM used for metals and alloys. The latter is more similar to welding in terms of equipment, but with many more 'welds'. The filler material can be added by wire or powder, and the process can take place in a protected atmosphere or vacuum. Contrary to this, the PBF process is based on a special powder-bed machine. The heat source is either an electron beam or a laser beam, and the build of a component takes place in a special chamber with a vacuum or a protective gas. The PBF comprises a significant number of layers of molten material, as the average powder particle size is approximately 50 μm.

The study begins with two sections introducing AM modelling. Simulating PBF and DED processes is computationally demanding because of the large number of 'welds', and the techniques used to reduce the computing time at the beginning of computational welding mechanics (CWM) developments are once again of interest. Therefore, a short section on CWM is included. Thereafter follows an update of an earlier review concerning finite element (FE) modelling of AM [1] based on the CWM approach [2,3]. References to more recent works are added, together with discussions about computational efficiency and defect estimation. The possibility to model defects, which is a significant challenge but also of great interest, is discussed at end of the study.

2. Summary of the computational welding mechanics approach

The overall aim of CWM is to establish methods and models that are usable for the control and design of welding processes to obtain appropriate mechanical performance of the welded component or structure [3]. The thermo-mechanical

* Corresponding author.
E-mail address: Lars-Erik.Lindgren@ltu.se (L.-E. Lindgren).

https://doi.org/10.1016/j.crme.2018.08.004
1631-0721/

Table 1
Modelling assumptions for various scopes of models.

Scale	Scope	Assumption/approach
Component	1. Minimum weight versus given load	Assume perfect process. Ideal geometry is obtained without any residual stresses, etc./Optimisation
	2. Tool path for DED process	Assume perfect process. Only considers motion of heat source/Optimisation
	3. Design support structure for PBF or evaluate residual stresses and deformations	Assume a residual state for each 'weld' which is accumulated to residual mechanical state of component
	4. Evaluate transient and residual state of component	CWM
	5. Evaluate microstructure	CWM with microstructure model
	6. Evaluate defects	CWM with additional models, see chapter 6
Process zone	7. Evaluate molten region	WPM including fluid flow of molten metal
	8. Evaluate beam–powder interaction	WPM including fluid flow of molten metal as well as powder particles
	9. Evaluate micro-structure, solidification details, grain structure, etc.	Models for representative volume elements/Phase field methods, etc.

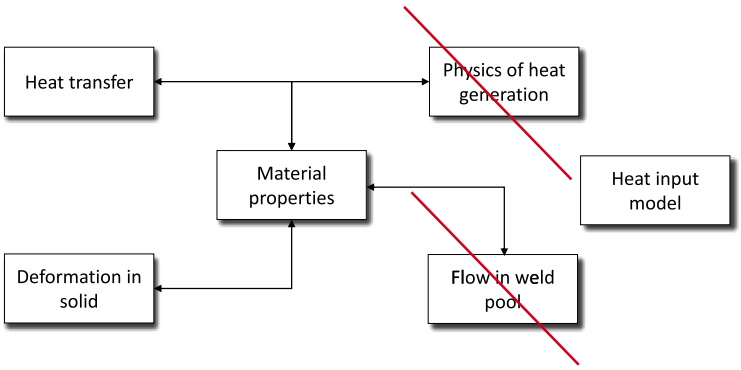

Fig. 1. Common modelling assumptions in CWM. Molten weld details are replaced by calibrated heat input model, and fluid flow is replaced by 'soft' elastic solid.

models can be combined with models for microstructure evolution, and thermo-metallurgical-mechanical interaction, as well as other features that enable the prediction of crack initiation. The description of heat generation requires only thermo-mechanics in the case of explosive welding, friction welding, or friction stir welding. However, resistance welding also requires the inclusion of the electrical field. However, the process becomes significantly more complex for fusion welding processes. Weld process modelling (WPM), levels 7 and 8 in Table 1, focuses on modelling the physics of the heat generation to predict heat distribution. The CWM models begin with a given heat input that replaces the details of the heat generation process, and utilises a heat input model where the heat distribution is prescribed, as shown in Fig. 1. This model must be calibrated or obtained from WPM models. The review in [1] contains more details about modelling and heat source models.

3. General modelling approaches for additive manufacturing

The required scope of the model decides the appropriate modelling approach, as described in Table 1. The focus in this study is on CWM models, as shown in levels 4–6 in Table 1. The CWM models have evolved significantly over the last 10 years, combining advanced dislocation density-based plasticity models with phase changes/precipitate models [1,4]. However, the great number of 'welds' in AM results in computational challenges, as will be discussed in the next section. The greatest modelling challenge for the future is the estimation of defect generation, about which little is known, and is discussed in chapter 6.

It can be seen from Table 1 that a macroscopic modelling approach cannot assist in choosing process parameters to obtain a stable process zone, as it does not, for instance, include the beam–powder interactions [5–7]. The CWM approach is more appropriate for determining the effect of the process on aspects including temperature, deformations, and microstructure. This is a consequence of excluding the physics of heat generation as well as fluid flow in the weld pool. The choice of process parameters requires an appropriate WPM. Although the focus of this study is on models, it is essential that the importance of experiments for better understanding, as well as model calibrations and validations, such as the NIST initiative AM-Bench (https://www.nist.gov/ambench), is not neglected.

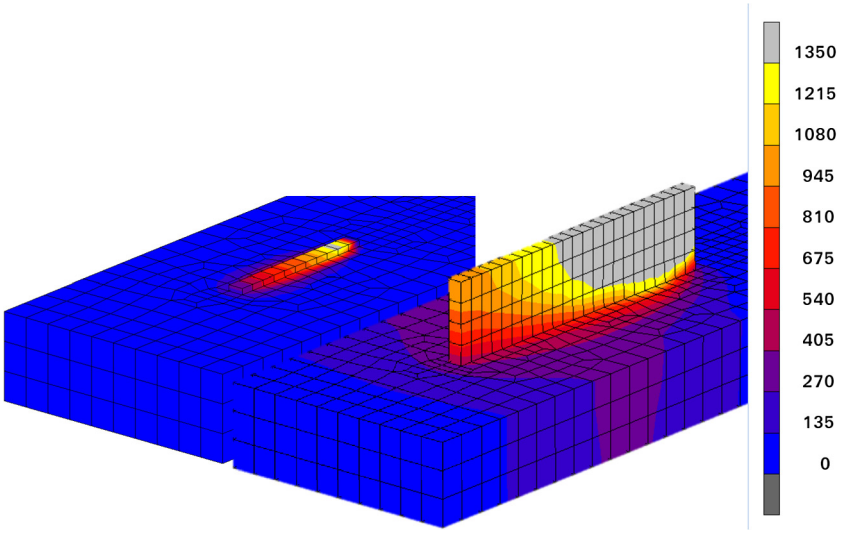

Fig. 2. History reduction by lumping of 'welds', with temperature fields shown. On the left is the case without lumping, and case on the right shows where 14 layers of 'welds' are added simultaneously, represented by four layers of elements [17]. The height of base plate is 12.7 mm.

4. Methods for efficiency

As indicated in Table 1, it is possible to perform simulations faster by introducing simplified modelling assumptions. The assumptions can be grouped into *spatial* and *temporal* reductions, or combinations thereof. A number of aspects regarding time and space are then ignored. A typical example of spatial reduction explores the possibility to reduce a 3D problem to a two-dimensional (2D) one [8,9]. This also implies a form of temporal reduction, as the axisymmetric model of a circumferential pipe and the use of a plane deformation model for a weld in a plate correspond to infinite welding speed. A temporal reduction ignores a portion of the history of the process or material response. The use of analytic solutions as well as solutions ignoring phase changes, lumping of 'welds', and similar simplifications are considered as temporal reductions, as shown in Fig. 2. It can be seen in Fig. 2 that the lumping also allows for the use of larger elements, which also speeds up the simulations. These approaches were adopted early in the CWM development [10]. The inherent strain approach, developed by Ueda et al. [11] in 1975, replaces the weld process by a measured final residual inelastic strain. The inherent strain field is approximated in a number of ways, depending on the approach taken. In order to be effective, this must typically be conducted in a more efficient way than a complete process simulation, which has limited the applicability of the approach. Having a representative inherent strain field enables a simple one-step analysis giving corresponding stresses and deformations of the component of the welded component [12]. This is one possible approach for level 6 in Table 1, and is used for AM in [13] by Keller and Ploshikhin. They used a small, fine-scale FE model of one hatch layer, which was analysed to obtain inherent strains that were applied for each layer in a macroscopic FE model. Michaleris et al. modified the approach, which became known as the decoupled plastic strain approach [14,15]. A similar simplification replacing the history of a 'weld' with a final state is described in [16]. Other approaches are available for replacing the final effect of a weld by simplified loading, for example in [9]. These simplifications were needed in the early days of CWM because of limited computing power, but are now being looked at again in the context of AM.

Assuming steady-state conditions and solving the thermomechanical problem for a moving coordinate system can be highly effective [18]. It can be considered to be a numerical technique, but is essentially a modelling assumption. Assuming steady-state conditions can be relevant for numerous weld cases, but less for AM processes at the component level. It is straightforward to implement for thermal fields, but the history dependency of the mechanical response requires tracing the history along 'streamlines', which complicates the implementation. Ding et al. [19,20] combined this for temperature fields with a number of sequentially analysed 2D plane-strain slices, each with a given temperature field along the weld path [21]. Therefore, each 2D model is subjected to an elasto-plastic analysis for each load step. Each slice gives the initial strain field to the next one. This could reduce the total simulation time by a factor of five for a simulated four-layer-high wall and still allow one to obtain a satisfactory residual state.

Another approach for efficient simulations is the use of a number of general *numerical techniques*, including parallel computing, adaptive meshing, sub-structuring, and element and solver technologies. A number of these techniques do not introduce approximations; however, some techniques introduce controllable errors, like remeshing. Montevecchi et al. [22] used independent remeshing in different zones and allowed for discontinuous, non-matching mesh between these zones to obtain an efficient grading of the mesh. They used a contact logic to enforce continuity in heat transfer and forces. Denlinger et al. [23] used remeshing to coarsen the mesh away from the heat source in order to solve an AM case, which reduced the computing time significantly. The use of remeshing with a continuous mesh is shown in Fig. 3. A fine layer of elements is used close to the heat source to resolve the gradients in this region, coarsening to larger elements in the layers further down.

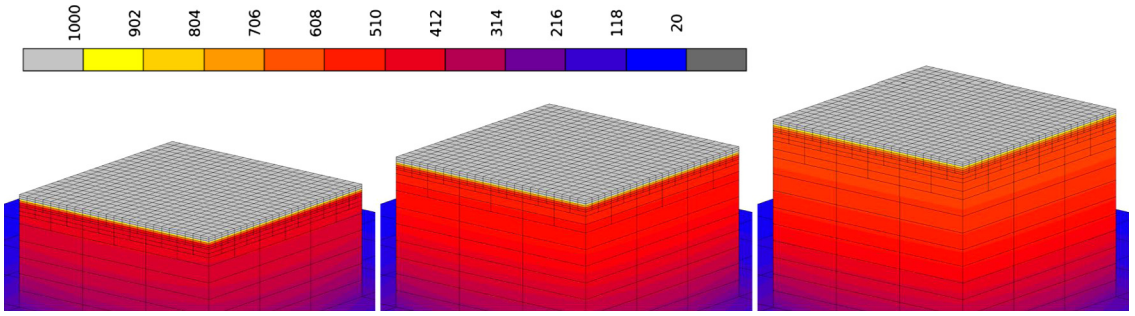

Fig. 3. Example of remeshing. Colours represent temperature fields. Rightmost one is a cube of $9 \times 9 \times 9$ mm.

5. Coupled thermomechanical CWM AM models

There are a number of well-established modelling approaches and notations in CWM, see [2]. One notation is cut-off temperature, which is used below. The exact meaning can vary, but the most common approach is to set it as the maximum temperature limit in mechanical analyses. Therefore, no changes in mechanical properties or thermal expansion are accounted for above this temperature. Modelling of materials subject to phase changes, like Ti-6Al-4V or low-alloy steels, requires specific procedures for accommodating the temperature-history-dependent properties. The most effective method is to combine a microstructure model with property models, which requires a type of homogenisation approach to obtain macroscopic material properties [1].

CWM models were applied to processes that became classified as AM later. The metal deposition cases in [24,25] are now denoted as AM. The example of repair welding of Alloy 718 described below is another example. A bulk of AM simulations are applied to DED processes, as the computational challenge is greater for PBF processes because of their significant difference in spatial scales [1].

Van Belle et al. [26] simulated PBF of stainless 15-5PH steel and limited the analysed volume to $0.6 \times 0.5 \times 0.5$ mm. The layer is 40 μm in thickness, and the spot diameter is 100 μm. They compared plane stress, plane strain, and 3D models, and concluded that the 3D option is necessary for optimising the process. They also evaluated the effect of removing effective plastic strain, i.e. strain hardening, at melting point versus at 1000 °C. They ignored phase changes in the alloy as well as rate effects on the plastic response of the material. Zaeh and Branner [27] computed residual stresses and deformation for selective laser melting. They ignored hatching and merged layers to enable the simulations by introducing 'scanning areas'. The structure was divided into 10 layers, each with a thickness of 1.0 mm. The actual layer thickness was 50 μm. They used separate material properties during heating and cooling to accommodate the effect of the phase transformations of the studied tool steel. They also accounted for transformation-induced plasticity. This approach was similar to the simplification of heating by Papadakis et al. [16].

Ding et al. [19,20] simulated DED with wire, which makes it possible to obtain increased build rates, but the residual stresses will also become greater [28]. The increased rates correspond to the addition of thicker layers. Therefore, the computing resources required for modelling are less demanding than for PBF, but remain significant. Their approach to increase the computational speed was discussed in the previous chapter. They simulated the addition four layers 2 mm in thickness, 5 mm in width, and 500 mm in length. They ignored phase changes in the structural steel and used a cut-off temperature of 1000 °C to avoid numerical problems. They also evaluated the effects of eight and 20 layers.

Montevecchi [22,29] simulated DED with wire, and modified the commonly used Goldak's double-ellipsoid heat source model [30] by adding heat from the molten filler itself to the weld. Approximately 50% of the total heat was obtained via the filler. They studied the 'one bead on plate' case, and one wall comprising five layers. They also ignored the effect of phase changes on the mechanical properties of the studied structural steel. The results obtained showed good agreement with the measurements.

Hodge et al. [31] simulated selected laser melting of austenitic, stainless steel AISI 316L. They used a lumping technique merging 20 layers into one, and performed validation field measurements of deformation and neutron diffraction measurements of elastic strains, obtaining good agreement between the results.

Heigel et al. [32] studied DED of Ti-6Al-4V using a temperature-dependent, but perfectly plastic flow, stress model. They applied a cut-off temperature of 800 °C and set all strain components to zero when reaching 690 °C. The AM process was a 62-layer-high wall, one deposit wide at each layer. The wall was 3 mm in width, 12.7 mm in height, and 38.1 mm in length. They compared their computational results with temperatures and deflections and reported a good correlation. Earlier simulations of DED of Ti-6Al-4V from the group are presented in [23,33]. They also modelled PBF of Ti-6Al-4V and Alloy 718 [34,35], and built cylindrical shapes with an outer diameter of 15.88 mm and a wall thickness of 1.59 mm, and a height up to 12.27 mm. Each layer was 50 μm in thickness and remeshing was applied to reduce the amount of required elements. It is of interest to note that the expected influence of hatching on asymmetry of the build did not manifest, indicating that ignoring hatching details when modelling could be feasible, at least for similar cases. Denlinger et al. [36] modelled laser PBF of Alloy 718, and could simulate 38 layers, as they utilised remeshing.

Yang et al. [37] simulated DED of Ti-6Al-4V with data from [32]. They simulated two walls 2.72 mm in width and 4.43 mm in height, one of which was 41.86 mm in length and the other 22.37 mm in length, and they formed a box. Five layers were added to reach 4.43 mm.

Vastola et al. [38] simulated one scan in PBF of Ti-6Al-4V to understand the relationship between process parameters and residual stresses. The model was sized $2.0 \times 1.5 \times 0.65$ mm. The layer's thickness was approximately 50 µm and the elements along the scan line were $62.5 \times 62.5 \times 12.5$ µm, and used different sets of properties representing melt, powder, and solid. The powder and the liquid had low yield strengths and were ideally plastic.

Cheng et al. [39] studied the effect of hatching on residual stresses. The selective laser melting process was applied on an Alloy 718 powder. The substrate was $8 \times 8 \times 1$ mm and the scanning islands were 6×6 mm. They simulated the addition of three layers of powders, each 30 µm in thickness. The elements utilised remeshing and the smallest elements were $200 \times 200 \times 15$ µm.

Marimuthu et al. [40] simulated the AM of a circular wall on a bent plate of Alloy 718, and used laser deposition of blown powder. The plate was $250 \times 250 \times 3$ mm and the height of the built wall varied between 20 and 28 mm because of the curvature of the support plate. The wall had a diameter of 100 mm, with a wall thickness of 25 mm. They lumped the deposition into five circular tracks divided into eight segments. One segmented track was added at a time, with a delay between each addition to obtain the correct total time for the process. Therefore, they activated a group of elements 40 times in the simulations.

Prabhakar et al. [41] modelled the PBF of Alloy 718 using an electron beam as a heat source. They added heat with each layer and modelled the build as 50 layers. The base plate had the dimensions $15 \times 15 \times 1$ cm, and each of the six built test coupons were $8 \times 1.8 \times 2$ cm.

Chiumenti et al. [42] simulated DED using an electron beam as a heat source and supplying Ti-6Al-4V as powder. The model was a more complex constitutive model than others, and included viscoplastic behaviour. They also simulated the thermal part of PBF of Ti-6Al-4V [43], and ignored the detailed resolution of hatching in favour of heating one or several layers simultaneously.

Li et al. [44,45] developed a three-step approach. A detailed thermal FE analysis provided a melt pool geometry and temperature field with high resolution. The analysed regions were $5 \times 0.6 \times 0.15$ mm, the first dimension being in the scan direction of the heat source, the second in the width direction, and the third in the thickness direction. The powder was supported by a substrate of size $5 \times 0.6 \times 5$ mm. The elements were sized $50 \times 50 \times 37.5$ µm. This initial analysis established a cross-sectional temperature field, with the unit normal to the direction of the velocity of the heat source. This field was used to construct a temperature field for a hatch, where all scans were parallel. This implies that the scans were performed simultaneously and would not affect each other. This obtained temperature field for a hatch region was applied on a larger $5 \times 5 \times 0.15$ mm FE mesh, with an additional 1 mm of solidified material of substrate below the powder giving a final thickness of 1.15 mm. The corresponding mechanical analysis was performed giving residual stresses for this medium scale. The deformation of a region of $35 \times 15 \times 0.15$ mm, with a support plate of $45 \times 22 \times 1$ mm, was then analysed by mapping residual stresses from the medium-sized model applied on each hatch region. This stress state is orientated according to the scan direction of each hatch region.

It is clear from the above studies that if a detailed analysis is required, it must be limited to small volumes. This is particularly true for PBF processes where each layer is 0.05 mm; however, the DED layers can be considerably thicker. Simulation of the state of components requires the use of temporal reductions, typically lumping of heating, as well as numerical methods like adaptive meshing. To date, numerous models have attempted to overcome these problems. However, they have placed less focus on the challenges in describing the material behaviour over a large temperature range, which at times involve phase changes.

6. Defect estimation

Introducing AM components in high-performance applications requires the control of defects. The results of numerous experimental studies have been published, particularly for aerospace alloys like Ti-6Al-4V and Alloy 718, which could lead to a renewed interest in modelling defects. Prediction of defects has not advanced significantly, despite the existence of CWM for several decades. However, the authors expect that the significant number of current joint efforts from multiple research areas will advance knowledge of failure prediction in the context of AM. The focus is on criteria for hot crack initiation used in welding and applicable to AM.

The use of the word 'estimate' indicates the statistical side of the problem. Defect initiation is a weakest link event, whereas plastic behaviour is more of an average property. Therefore, the scatter is greater when considering defects. The initiation of a defect is a combination of macroscopic mechanical loading as well as other factors, including the existence of sensitive microstructures, pores, and inclusions [46–48]. The macroscopic load is from the accumulated effect of thermal strains, including solidification shrinkage and mechanical restraints from the material itself, and possible fixturing.

Weld cracking can be grouped into hot cracking, solid-state cracking, and the special cases of hydrogen-induced and stress-corrosion cracking. The latter two are assigned their own categories, although they appear in the solid-state material. Hot cracking comprises solidification cracking and liquation cracking. The former initiates in the liquid films, between the growing dendrites from the growing grains, during solidification. It has a solidification range dependent on its alloying composition. Therefore, cracking is more likely for material with a large solidification range, which can be extended because

of segregation. Liquation cracking is similar, but occurs in the partially melted zone, in the brittle temperature range (BTR) of the material. Solid-state cracking comprises ductility dip cracking, reheat cracking, and lamellar cracking. It will not be discussed here, and details can be found in [47].

There are criteria that are more or less based on the underlying physics of crack initiation and growth. They are discussed in the following sections, from the less to the more complex criteria.

6.1. Thermal-based criteria

Crack initiation requires mechanical loading, as discussed earlier, but pure thermal criteria may sometimes be sufficient. Mukherjee et al. [49,50] summarised dimensionless numbers, which can characterise a process, like a non-dimensional heat input that is correlated to the lack of fusion when small, or pores due to key hole when greater. The use of these criteria is highly complex because of the strongly non-linear and complex conditions of AM. Beuth et al. [51,52] used the Rosenthal analytic solution for the temperature field to characterise the process, and generated non-dimensional process maps of power versus speed with the lower limit against lack of fusion and upper limit against pores. King et al. [53] used normalised enthalpy as a measure of the risk for key-holing leading to pores. The Rosenthal analytic solution was also used to estimate the width of the molten pool in order to have sufficient overlap between scans [54]. Cooling rates are an important parameter, and affect the formation of Laves in Alloy 718 [55] and segregation [56]. They, in turn, affect the risk of cracking [57], which is discussed in the chapter on modelling AM of Alloy 718.

6.2. Thermomechanical-based criteria

The previous thermal criteria emphasised the importance of temperature history for the microstructure, but also indirectly included the straining of the material, therefore requiring only a thermal analysis. However, a thermomechanical simulation makes it possible to directly include the mechanical load. Various criteria have been applied to a given structure and utilised in welding simulations, and the structure was characterised by a temperature range. The temperature range depends on metallurgy, so the criteria could also be denoted as metallurgy-informed. The BTR is the typical range choice. Critical stress criteria relate the stress over the liquid film to the maximum stress it can sustain, whereas it is more common to use critical strain [58]. Jonsson et al. [59] evaluated the accumulated plastic strain when the material cooled from 1400 °C to 1000 °C. The range was chosen based on the extended solidification range of steel owing to the segregation of sulphur. This criterion showed a good correlation with the observed crack locations in a butt-welded plate. Wei et al. [60–62] used a similar approach for the accumulated mechanical strain in the BTR. They used a temperature of approximately 1275 °C as the lower limit of BTR, which can be the coherency temperature [58]. Bergmann and Hilbinger [63] assumed that the solidification shrinkage is compensated by backfill from the melt until an accumulated strain of 0.02 was reached in the solidification temperature range. This value was obtained by fitting versus test.

6.3. Metallurgy and fluid flow informed criteria

The previous models circumvented details about the physics of the process, and ignored the important aspects of the liquid film, its thickness, as well as the backflow of liquid from melt. The model proposed by Rappaz et al. [64] for casting the RDG model yields the pressure in the film and assumes that decreasing pressure leads to cavitation and fracture initiation. However, the model requires considerable underpressure for cavitation. Drezet and Allehaux [65] applied the model to welding. Coniglio and Cross [58,66] used the RDG model combined with strain localisation over the liquid film, and assumed pre-existing pores leading to realistic underpressures for cavitation. Kou [46] described this model as well as other ones, including his own developments which accounted for the effect of strain rates. On-going work [67–69] combines the RDG model with developments by Coniglio, and additional developments to calculate the length of the frozen weld in initial cracks in the weld metal, and is discussed in the next chapter. The driving temperature and stress/strain fields are obtained from FE simulations of the weld process.

7. Thermo-metallurgical-mechanical simulation of AM of Alloy 718

The use of FE modelling of AM for a critical aerospace material, Alloy 718, is discussed below. It is repair welding or DED with wire using the notations of AM. The model combines a microstructure and constitutive model for the flow stress. The possibility to also include defect estimates is illustrated for Alloy 718.

Alloy 718 is commonly used aerospace material with significant high-temperature properties as well as weldability. However, micro-fissures from liquation cracking have been observed [70,71]. Wang et al. [72] reviewed the use of PBF processing of Alloy 718. The AM-produced components can also have pores, unmolten powders, and bonding defects from the PBF process.

The repair welding of Alloy 718, followed by an ageing treatment by induction heating, was simulated [73,74]. The dislocation density-based plasticity model, as shown in Fig. 4, accounts for the rate-dependent behaviour, dynamic, and static recovery and the effect of the γ''-precipitate size distribution. There are no precipitates in the annealed state, and there is approximately 13% volume fraction in the fully aged state.'

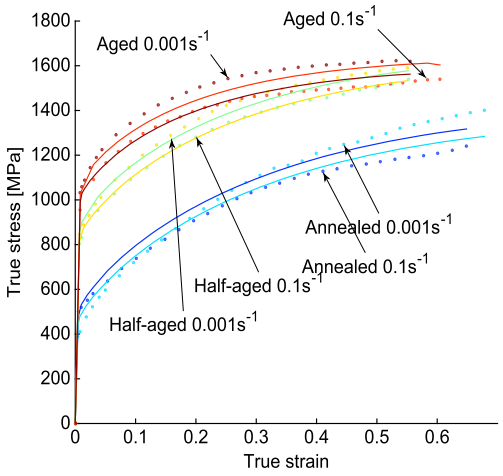

Fig. 4. Examples of measured and computed flow stress curves of Alloy 718.

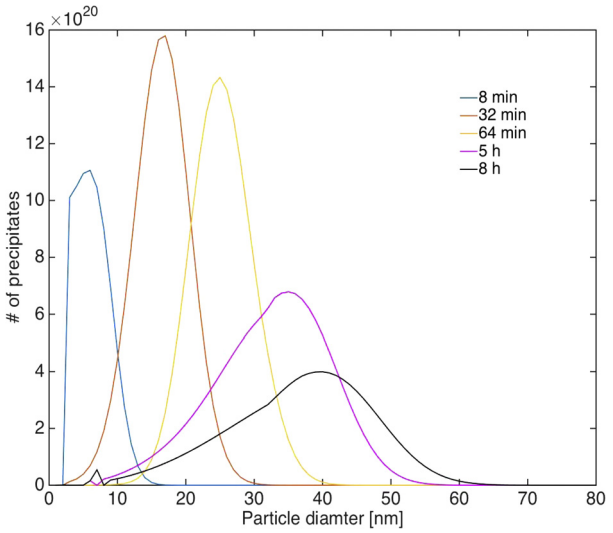

Fig. 5. γ''-precipitate size distribution for various ageing times at 750 °C.

The flow stress model is combined with a precipitate model based on the classical nucleation and growth theory [75,76]. An example of the computed results is shown in Fig. 5.

Fig. 6 shows the results from the simulation of the repair welding. The AM-produced Alloy 718 components can also have pores, unmolten powders, and bonding defects from the PBF process. Higher cooling rates reduce the amount of Laves phases and segregation of Nb.

Draxler et al. [67–69] developed a hot crack initiation criterion based on frozen weld in pores in the liquid film between grain boundaries during solidification, as shown in Fig. 7. This is a Varestraint test where the heat source is moving towards the right. The figure is plotted 0.1 s after bending of the welded plate is completed, when the heat source is at $x = 41.6$ mm.

The curved lines follow the gradient of the temperature field and outline the liquid films between the grains. The solidification starts from the dashed line, denoting the fusion zone. The rightmost liquid film has just started to solidify at the shown instance. Their locations are arbitrarily chosen in the post-processing of the welding simulation. This post-processing combines FE results, including thermal and mechanical fields with a one-dimensional non-linear pressure model, and more detailed information about properties in and near the liquid film to obtain information about the risk of crack initiation. The computed underpressure is related to a critical pore size that could remain when the film is completely solidified because then it cannot still be healed by liquid backflow.

8. Discussion

The review of selected publications concerning the use of the CWM modelling approach applied to AM highlights a number of issues for the future. Most studies showed the need for computational efficiency and focused on various ap-

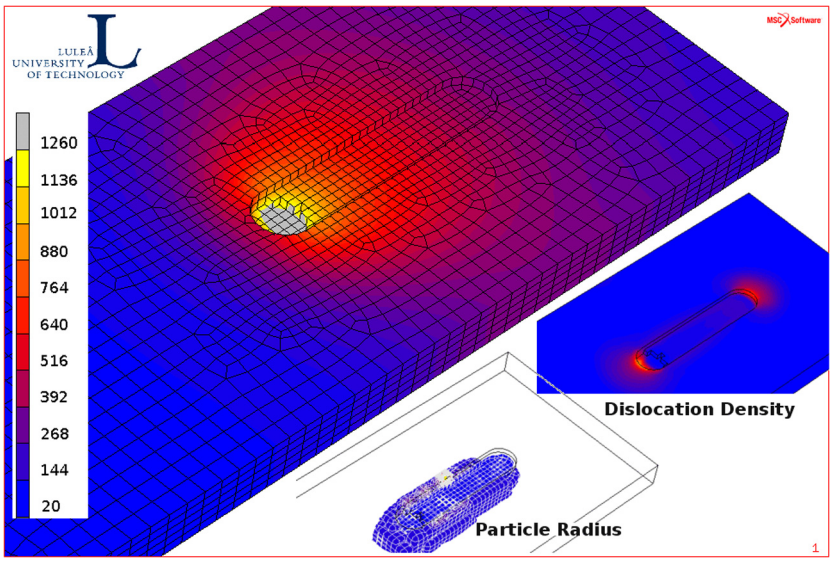

Fig. 6. Temperature field, dislocation density, and precipitate mean size during repair welding of Alloy 718.

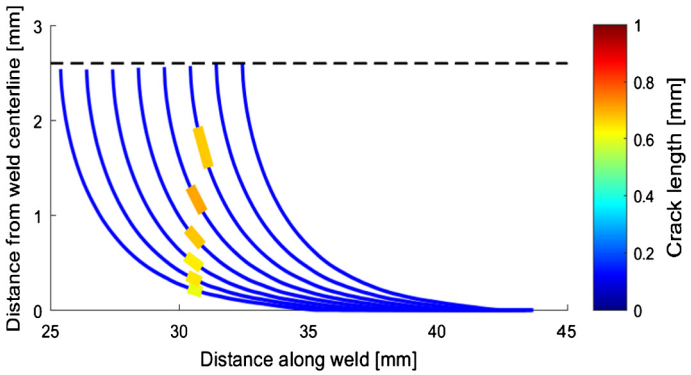

Fig. 7. Length of initiated cracks in welded Alloy 718. Results obtained from post-processing of finite element simulation of Varestraint test. Heat source moves along the *x*-axis towards the right.

proaches to speed up simulations while obtaining sufficiently accurate results. The studies showed that accurate results can be obtained through the effective use of experimental results. Future developments could include efficient methods with overall good accuracies for the deformation behaviour on a component scale in conjunction with detailed models showing microstructures, as well as defect information for the selected regions of components.

The current focus on efficiency in AM modelling is probably the reason why the effect of phase changes has been ignored or simplified. Furthermore, we anticipate a continuous improvement in material modelling necessary for detailed models.

Experimental results supporting both the understanding of the physics as well as calibration and validation of models will continue to be important. This is a problem for PBF processes taking place in closed chambers.

Acknowledgement

This research was supported by the Swedish Foundation for Strategic Research project ‘Development of Process and Material in Additive Manufacturing’, Reference number GMT14-0048.

References

[1] L.-E. Lindgren, A. Lundbäck, M. Fisk, R. Pederson, J. Andersson, Simulation of additive manufacturing using coupled constitutive and microstructure models, Addit. Manuf. 12 (2016) 144–158.
[2] L.-E. Lindgren, Computational Welding Mechanics: Thermomechanical and Microstructural Simulations, Woodhead Publishing, 2007.
[3] L.E. Lindgren, Numerical modelling of welding, Comput. Methods Appl. Mech. Eng. 195 (2006) 6710–6736.
[4] L.-E. Lindgren, A. Lundbäck, M. Fisk, Thermo-mechanics and microstructure evolution in manufacturing simulations, J. Therm. Stresses 36 (2013) 564–588.
[5] A.V. Gusarov, I. Smurov, Modeling the interaction of laser radiation with powder bed at selective laser melting, Phys. Proc. 5B (2010) 381–394.

[6] Y.S. Lee, W. Zhang, Modeling of heat transfer, fluid flow and solidification microstructure of nickel-base superalloy fabricated by laser powder bed fusion, Addit. Manuf. 12 (2016) 178–188, part B.
[7] A. Foroozmehr, M. Badrossamay, E. Foroozmehr, S.i. Golabi, Finite element simulation of selective laser melting process considering optical penetration depth of laser in powder bed, Mater. Des. 89 (2016) 255–263.
[8] L.-E. Lindgren, Finite element modelling and simulation of welding, part 1 increased complexity, J. Therm. Stresses 24 (2001) 141–192.
[9] P. Michaleris, Z. Feng, G. Campbell, Evaluation of 2D and 3D FEA models for predicting residual stress and distortion, in: Approximate Methods in the Design and Analysis of Pressure Vessels and Piping Components, in: Pressure Vessels and Piping Division (Publication) PVP, vol. 347, American Society of Mechanical Engineers, 1997, pp. 91–102.
[10] E.F. Rybicki, R.B. Stonesifer, Computation of residual stresses due to multipass welds in piping systems, J. Press. Vessel Technol. 101 (1979) 149–154.
[11] Y. Ueda, K. Fukuda, K. Nakacho, S. Endo, A new measuring method of residual stresses with the aid of finite element method and reliability of estimated values (in Japanese), J. Soc. Nav. Archit. Jpn. 1975 (1975) 499–507.
[12] D. Deng, H. Murakawa, W. Liang, Numerical simulation of welding distortion in large structures, Comput. Methods Appl. Mech. Eng. 196 (2007) 4613–4627.
[13] N. Keller, V. Ploshikhin, New method for fast predictions of residual stress and distortion of AM parts, in: Annual International Solid Freeform Fabrication Symposium—An Additive Manufacturing Conference, University of Texas, Austin, USA, 2014.
[14] P. Michaleris, L. Zhang, S.R. Bhide, P. Marugabandhu, Evaluation of 2D, 3D and applied plastic strain methods for predicting buckling welding distortion and residual stress, Sci. Technol. Weld. Join. 11 (2006) 707–716.
[15] P. Michaleris, A. DeBiccari, Prediction of welding distortion, Weld. J. 76 (1997) 172s–181s.
[16] L. Papadakis, A. Loizou, J. Risse, S. Bremen, J. Schrage, A computational reduction model for appraising structural effects in selective laser melting manufacturing, Virtual Phys. Prototyping 9 (2014) 17–25.
[17] A. Malmelöv, Modeling of Additive Manufacturing with Reduced Computational Effort, Engineering Sciences and Mathematics, Luleå University of Technology, Luleå, 2016.
[18] J. Shanghvi, P. Michaleris, Thermo-elasto-plastic finite element analysis of quasi-state processes in Eulerian reference frames, Int. J. Numer. Methods Eng. 53 (2002) 1533–1556.
[19] J. Ding, P. Colegrove, J. Mehnen, S. Williams, F. Wang, P.S. Almeida, A computationally efficient finite element model of wire and arc additive manufacture, Int. J. Adv. Manuf. Technol. 70 (2014) 227–236.
[20] J. Ding, P. Colegrove, J. Mehnen, S. Ganguly, P.M. Sequeira Almeida, F. Wang, S. Williams, Thermo-mechanical analysis of wire and arc additive layer manufacturing process on large multi-layer parts, Comput. Mater. Sci. 50 (2011) 3315–3322.
[21] P. Colegrove, C. Ikeagu, A. Thistlethwaite, S. Williams, T. Nagy, W. Suder, A. Steuwer, T. Pirling, Welding process impact on residual stress and distortion, Sci. Technol. Weld. Join. 14 (2009) 717–725.
[22] F. Montevecchi, G. Venturini, N. Grossi, A. Scippa, G. Campatelli, Finite element mesh coarsening for effective distortion prediction in wire arc additive manufacturing, Addit. Manuf. 18 (2017) 145–155.
[23] E.R. Denlinger, J. Irwin, P. Michaleris, Thermomechanical modeling of additive manufacturing large parts, J. Manuf. Sci. Eng. 136 (2014) 061007.
[24] A. Lundbäck, L.-E. Lindgren, Modelling of metal deposition, Finite Elem. Anal. Des. 47 (2011) 1169–1177.
[25] M. Chiumenti, M. Cervera, A. Salmi, C. Agelet de Saracibar, N. Dialami, K. Matsui, Finite element modeling of multi-pass welding and shaped metal deposition processes, Comput. Methods Appl. Mech. Eng. 199 (2010) 2343–2359.
[26] L. Van Belle, G. Vansteenkiste, J.C. Boyer, Comparisons of numerical modelling of the selective laser melting, Key Eng. Mater. 504–506 (2012) 1067–1072.
[27] M.F. Zaeh, G. Branner, Investigations on residual stresses and deformations in selective laser melting, Prod. Eng. 4 (2010) 35–45.
[28] D. Ding, Z. Pan, D. Cuiuri, H. Li, Wire-feed additive manufacturing of metal components: technologies, developments and future interests, Int. J. Adv. Manuf. Technol. 81 (2015) 465–481.
[29] F. Montevecchi, G. Venturini, A. Scippa, G. Campatelli, Finite element modelling of wire-arc-additive-manufacturing process, Proc. CIRP 55 (2016) 109–114.
[30] J. Goldak, A. Chakravarti, M. Bibby, A new finite element model for welding heat sources, Metall. Trans. B 15B (1984) 299–305.
[31] N.E. Hodge, R.M. Ferencz, R.M. Vignes, Experimental comparison of residual stresses for a thermomechanical model for the simulation of selective laser melting, Addit. Manuf. 12 (2016) 159–168, part B.
[32] J.C. Heigel, P. Michaleris, E.W. Reutzel, Thermo-mechanical model development and validation of directed energy deposition additive manufacturing of Ti-6Al-4V, Addit. Manuf. 5 (2015) 9–19.
[33] E.R. Denlinger, J.C. Heigel, P. Michaleris, Residual stress and distortion modeling of electron beam direct manufacturing Ti-6Al-4V, Proc. Inst. Mech. Eng., B J. Eng. Manuf. 229 (2015) 1803–1813.
[34] A.J. Dunbar, E.R. Denlinger, M.F. Gouge, P. Michaleris, Experimental validation of finite element modeling for laser powder bed fusion deformation, Addit. Manuf. 12 (2016) 108–120.
[35] A.J. Dunbar, E.R. Denlinger, M.F. Gouge, T.W. Simpson, P. Michaleris, Comparisons of laser powder bed fusion additive manufacturing builds through experimental in situ distortion and temperature measurements, Addit. Manuf. 15 (2017) 57–65.
[36] E.R. Denlinger, M. Gouge, J. Irwin, P. Michaleris, Thermomechanical model development and in situ experimental validation of the laser powder-bed fusion process, Addit. Manuf. 16 (2017) 73–80.
[37] Q. Yang, P. Zhang, L. Cheng, Z. Min, M. Chyu, A.C. To, Finite element modeling and validation of thermomechanical behavior of Ti-6Al-4V in directed energy deposition additive manufacturing, Addit. Manuf. 12 (2016) 169–177.
[38] G. Vastola, G. Zhang, Q.X. Pei, Y.W. Zhang, Controlling of residual stress in additive manufacturing of Ti6Al4V by finite element modeling, Addit. Manuf. 12 (2016) 231–239, part B.
[39] B. Cheng, S. Shrestha, K. Chou, Stress and deformation evaluations of scanning strategy effect in selective laser melting, Addit. Manuf. 12 (2016) 240–251, part B.
[40] S. Marimuthu, D. Clark, J. Allen, A.M. Kamara, P. Mativenga, L. Li, R. Scudamore, Finite element modelling of substrate thermal distortion in direct laser additive manufacture of an aero-engine component, Proc. Inst. Mech. Eng., Part C, J. Mech. Eng. Sci. 227 (2012) 1987–1999.
[41] P. Prabhakar, W.J. Sames, R. Dehoff, S.S. Babu, Computational modeling of residual stress formation during the electron beam melting process for Inconel 718, Addit. Manuf. 7 (2015) 83–91.
[42] M. Chiumenti, M. Cervera, N. Dialami, B. Wu, L. Jinwei, C. Agelet de Saracibar, Numerical modeling of the electron beam welding and its experimental validation, Finite Elem. Anal. Des. 121 (2016) 118–133.
[43] M. Chiumenti, E. Neiva, E. Salsi, M. Cervera, S. Badia, J. Moya, Z. Chen, C. Lee, C. Davies, Numerical modelling and experimental validation in selective laser melting, Addit. Manuf. 18 (2017) 171–185.
[44] C. Li, J.F. Liu, X.Y. Fang, Y.B. Guo, Efficient predictive model of part distortion and residual stress in selective laser melting, Addit. Manuf. 17 (2017) 157–168.
[45] C. Li, C.H. Fu, Y.B. Guo, F.Z. Fang, A multiscale modeling approach for fast prediction of part distortion in selective laser melting, J. Mater. Process. Technol. 229 (2016) 703–712.

[46] S. Kou, A simple index for predicting the susceptibility to solidification cracking, Weld. J. 94 (2015) 374s–388s.
[47] J. Lippold, Welding Metallurgy and Weldability, John Wiley & Sons, Hoboken, New Jersey, 2015.
[48] C.E. Cross, N. Coniglio, Weld solidification cracking: critical conditions for crack initiation and growth, in: T. Böllinghaus, H. Herold, C.E. Cross, J.C. Lippold (Eds.), Hot Cracking Phenomena in Welds II, Springer Berlin Heidelberg, Berlin, Heidelberg, 2008, pp. 47–66.
[49] T. Mukherjee, J.S. Zuback, A. De, T. DebRoy, Printability of alloys for additive manufacturing, Sci. Rep. 6 (2016) 19717.
[50] T. Mukherjee, V. Manvatkar, A. De, T. DebRoy, Dimensionless numbers in additive manufacturing, J. Appl. Phys. 121 (2017) 064904.
[51] D. Rosenthal, Mathematical theory of heat distribution during welding and cutting, Weld. J. 20 (1941) 220s–234s.
[52] D. Rosenthal, The theory of moving sources of heat and its application to metal treatments, Trans. Amer. Soc. Mech. Eng. 68 (1946) 849–866.
[53] W.E. King, H.D. Barth, V.M. Castillo, G.F. Gallegos, J.W. Gibbs, D.E. Hahn, C. Kamath, A.M. Rubenchik, Observation of keyhole-mode laser melting in laser powder-bed fusion additive manufacturing, J. Mater. Process. Technol. 214 (2014) 2915–2925.
[54] M. Tang, P.C. Pistorius, J.L. Beuth, Prediction of lack-of-fusion porosity for powder bed fusion, Addit. Manuf. 14 (2017) 39–48.
[55] S.G.K. Manikandan, D. Sivakumar, K.P. Rao, M. Kamaraj, Effect of weld cooling rate on Laves phase formation in Inconel 718 fusion zone, J. Mater. Process. Technol. 214 (2014) 358–364.
[56] C.H. Radhakrishna, K. Prasad Rao, The formation and control of Laves phase in superalloy 718 welds, J. Mater. Sci. 32 (1997) 1977–1984.
[57] R.G. Thompson, D.E. Mayo, B. Radhakrishnan, The relationship between carbon content, microstructure, and intergranular liquation cracking in cast nickel Alloy 718, Metall. Trans. A 22 (1991) 557–567.
[58] N. Coniglio, C.E. Cross, Initiation and growth mechanisms for weld solidification cracking, Int. Mater. Rev. 58 (2013) 375–397.
[59] M. Jonsson, L. Karlsson, L.-E. Lindgren, Thermal stresses, plate motion and hot cracking in butt-welding, in: 4th International Conference on Mechanical Behaviour of Materials, Stockholm, Sweden, 1983, pp. 273–279.
[60] Y. Wei, Z. Dong, R. Liu, Z. Dong, Y. Pan, Simulating and predicting weld solidification cracks, in: T. Böllinghaus, H. Herold (Eds.), Hot Cracking Phenomena in Welds, Springer Berlin Heidelberg, Berlin, Heidelberg, 2005, pp. 185–222.
[61] Y.H. Wei, Z.B. Dong, R.P. Liu, Z.J. Dong, Three-dimensional numerical simulation of weld solidification cracking, Model. Simul. Mater. Sci. Eng. 13 (2005) 437–454.
[62] Y. Wei, Z. Dong, R. Liu, Z. Dong, Modeling the Trans-Varestraint test with finite element method, Comput. Mater. Sci. 35 (2006) 84–91.
[63] H. Bergmann, R. Hilbinger, Numerical simulation of centre line hot cracks in laser beam welding of aluminium close to the sheet edge, in: H. Cerjak (Ed.), Mathematical Modelling of Weld Phenomena 4, The Institute of Materials, Graz, Austria, 1998, pp. 658–668.
[64] M. Rappaz, J.M. Drezet, M. Gremaud, A new hot-tearing criterion, Metall. Mater. Trans. A 30 (1999) 449–455.
[65] J.M. Drezet, D. Allehaux, Application of the Rappaz–Drezet–Gremaud hot tearing criterion to welding of aluminium alloys, in: T. Böllinghaus, H. Herold, C.E. Cross, J.C. Lippold (Eds.), Hot Cracking Phenomena in Welds II, Springer Berlin Heidelberg, Berlin, Heidelberg, 2008, pp. 27–45.
[66] N. Coniglio, C.E. Cross, Mechanisms for solidification crack initiation and growth in aluminum welding, Metall. Mater. Trans. A 40 (2009) 2718–2728.
[67] J. Draxler, J. Edberg, L.-E. Lindgren, J. Andersson, Simulation of hot cracking in superalloys. Part III. Application on Varestraint tests of Alloy 718, submitted for publication.
[68] J. Draxler, J. Edberg, L.-E. Lindgren, J. Andersson, Simulation of hot cracking in superalloys. Part II. Model for pressure in grain boundary liquid film, submitted for publication.
[69] J. Draxler, J. Edberg, L.-E. Lindgren, J. Andersson, Simulation of hot cracking in superalloys. Part I. Pore based crack criterion, submitted for publication.
[70] D. Clark, M.R. Bache, M.T. Whittaker, Shaped metal deposition of a nickel alloy for aero engine applications, J. Mater. Process. Technol. 203 (2008) 439–448.
[71] J.K. Hong, J.H. Park, N.K. Park, I.S. Eom, M.B. Kim, C.Y. Kang, Microstructures and mechanical properties of Inconel 718 welds by CO2 laser welding, J. Mater. Process. Technol. 201 (2008) 515–520.
[72] X. Wang, X. Gong, K. Chou, Review on powder-bed laser additive manufacturing of Inconel 718 parts, Proc. Inst. Mech. Eng., B J. Eng. Manuf. 231 (2016) 1890–1903.
[73] M. Fisk, Validation of induction heating model for Alloy 718 components, Int. J. Comput. Methods Eng. Sci. Mech. 12 (2011) 161–167.
[74] M. Fisk, A. Lundbäck, Simulation and validation of repair welding and heat treatment of an Alloy 718 plate, Finite Elem. Anal. Des. 58 (2012) 66–73.
[75] M. Fisk, J.C. Ion, L.E. Lindgren, Flow stress model for IN718 accounting for evolution of strengthening precipitates during thermal treatment, Comput. Mater. Sci. 82 (2014) 531–539.
[76] M. Fisk, A. Lundbäck, J. Edberg, J.M. Zhou, Simulation of microstructural evolution during repair welding of an IN718 plate, Finite Elem. Anal. Des. 120 (2016) 92–101.